Materials Letters 62 (2008) 4545–4548

Contents lists available at ScienceDirect

Materials Letters

journal homepage: www.elsevier.com/locate/matlet

# Preparation of highly ordered Fe-SBA-1 and Ti-SBA-1 cubic mesoporous silica via sol-gel processing of silatrane

Walairat Tanglumlert [a], Toyoko Imae [b], Timothy J. White [c], Sujitra Wongkasemjit [a,*]

[a] The Petroleum and Petrochemical College, Chulalongkorn University, Bangkok 10330, Thailand
[b] Graduate School of Science and Technology, Keio University, Yokohama 223-8522, Japan
[c] School of Materials Science and Engineering, Nanyang Technological University, Singapore

ARTICLE INFO

*Article history:*
Received 26 May 2008
Accepted 21 August 2008
Available online 24 August 2008

*Keywords:*
Silatrane
Mesoporous silica
SBA-1
Cubic phase
Sol-gel process

ABSTRACT

Silatrane prepared from fumed silica and triethanolamine (TEA) was used as a precursor for the sol-gel synthesis of M-SBA-1 (M=Fe and Ti) at room temperature using cetyltrimethylammonium bromide as a template, and dilute solutions of ferric chloride and titanium glycolate as metal sources. Powder X-ray diffraction (XRD) showed the mesoporous materials to be well-ordered cubic structures, while $N_2$ adsorption/desorption measurements yielded high surface areas. Diffuse reflectance UV–visible spectroscopy demonstrated that iron ($Fe^{3+}$) and titanium ($Ti^{4+}$) were incorporated in the framework of the calcined materials to loadings of 6 wt.% Fe and 10 wt.% Ti without perturbing the ordered mesoporous structure.


## 1. Introduction

In mesoporous materials of the SBA family, phases with a three-dimensional pore system are advantageous for catalytic applications, compared to one-dimensional pore arrays, because of the thicker walls, greater pore diameters and improved hydrothermal stability with respect to reference materials such as MCM-41 [1–3]. Moreover, metal substituted mesoporous architectures are attractive for catalytic reactions involving molecules that are sterically excluded from the channels of microporous zeolites [4–6]. Recently, several metal ions including $Ti^{4+}$, $Cr^{6+}$, $Mo^{5+}$, $V^{5+}$ and $Fe^{3+}$ have been successfully incorporated into the frameworks of mesoporous silicas [7–11]. In particular, Ti-substituted molecular sieves ($Ti^{4+}$), such as TS-1, Ti-beta and Ti-MCM-41 have displayed excellent catalytic properties in selective oxidation reactions when using aqueous hydrogen peroxide as the oxidant [12–14]. Iron-containing mesoporous materials ($Fe^{3+}$), such as Fe-SBA-1, Fe-MCM-41, and Fe-HMS have also been extensively studied because of their unique catalytic enhancement of hydrocarbon oxidation, selective reduction, acylation and alkylation reactions [2,3].

In an earlier report, the successful synthesis of SBA-1 mesoporous silica via a sol-gel process using silatrane was described [15]. Here, this approach is extended to the preparation of highly ordered M-SBA-1 (M=Fe and Ti) cubic mesoporous silicas, and the structural and physical properties of these materials evaluated.

## 2. Methodology

### 2.1. Materials

Fumed silica ($SiO_2$, 99.8%) (Sigma-Aldrich), titanium dioxide ($TiO_2$) (Carlo Erba), triethanolamine (TEA) (Carlo Erba), tetraethylenetriamine (TETA) (FACAI, Thailand), ethylene glycol (J.T. Baker, USA), acetronitrile (Labscan, Asia), ferric chloride ($FeCl_3$) (Sigma-Aldrich), hexadodecyltrimethylammonium bromide ($C_{16}$TMAB) (Sigma-Aldrich), $H_2SO_4$ (Labscan, Asia) and NaOH (Labscan, Asia) were used without treatment.

### 2.2. Preparation of mesoporous M-SBA-1

In this synthesis, solution A was prepared by adding $C_{16}$TMAB (0.44 g) to water (30 ml) and stirring for 0.5 h to obtain a clear solution. Solution B was prepared by dissolving silatrane precursor (5 mmol, 1.4 g), synthesized following the procedure described in references [16], in 14 ml of 0.3 M $H_2SO_4$ and NaOH (1.7 mmol, 0.068 g) by stirring for 0.5 h. The required amount of metal precursor, titanium glycolate synthesized according to Ref. [17], or $FeCl_3$, was added to solution B and stirring continued for 0.5 h. Solution B was then added to the solution A under vigorous stirring that continued for 4 h. Water

* Corresponding author. Tel.: +66 2 218 4133; fax: +66 2 215 4459.
*E-mail address:* dsujitra@chula.ac.th (S. Wongkasemjit).

0167-577X/$ – see front matter © 2008 Elsevier B.V. All rights reserved.
doi:10.1016/j.matlet.2008.08.030

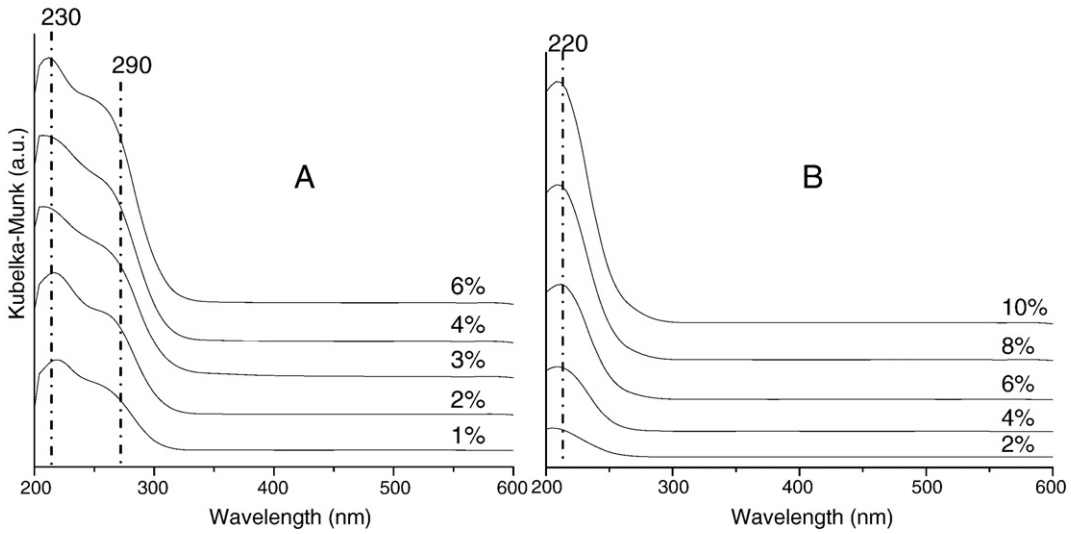


**Fig. 1.** Diffuse reflectance UV–visible spectra of calcined Fe-SBA-1 (A) and Ti-SBA-1 (B) mesoporous materials as a function of incorporated metal loading in the framework.

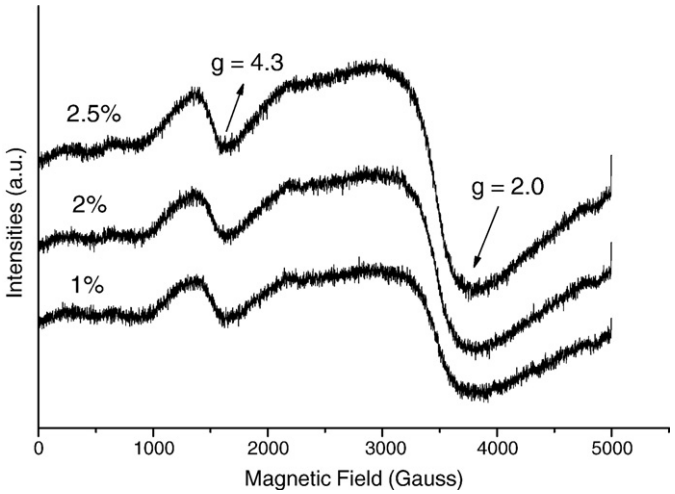


**Fig. 2.** ESR spectra of calcined Fe-SBA-1 materials of different iron content.

(30 ml) was added to this mixture before aging for 2 days at room temperature to form a white precipitate. The product was filtered, washed with distilled water, and dried at room temperature overnight. The template was removed by calcination (560 °C/6 h) in a Carbolite Furnace (CFS 1200) at a heating rate of 0.5 °C/min.

### *2.3. Characterization*

The mesoporous products were characterized using a Rigaku X-ray diffractometer (XRD) with patterns accumulated at a scan speed of 1°/s using CuKα radiation over the range of $2\theta$=1.5–8°. M-SBA-1 mesopore order was directly examined using a JEOL 2010F transmission electron microscope (TEM). Specific surface area and average pore size were determined by the Brunauer–Emmett–Teller (BET) method with a Quantasorb JR instrument. Diffuse reflectance UV–visible spectroscopic measurements were recorded on a Shimadzu UV-2550 spectrometer fitted with an ISR-2200 integrating sphere attachment from 200–600 nm referenced to $BaSO_4$. Electron spin resonance (ESR) spectra were measured at the X-band, ~9 GHz, on a JEOL JES-RE2X spectrometer.

## 3. Results and discussion

Higher metal ($Ti^{4+}$, $Fe^{3+}$) incorporation in SBA-1 has been attributed to a surfactant silica assembly mechanism, in which the mesophase forms under acidic conditions via an $S^+X^-I^+$ pathway (S, X and I correspond to surfactant, halide and inorganic species, respectively). As silatrane is a water soluble alkoxide, hydrolysis to silicate generates

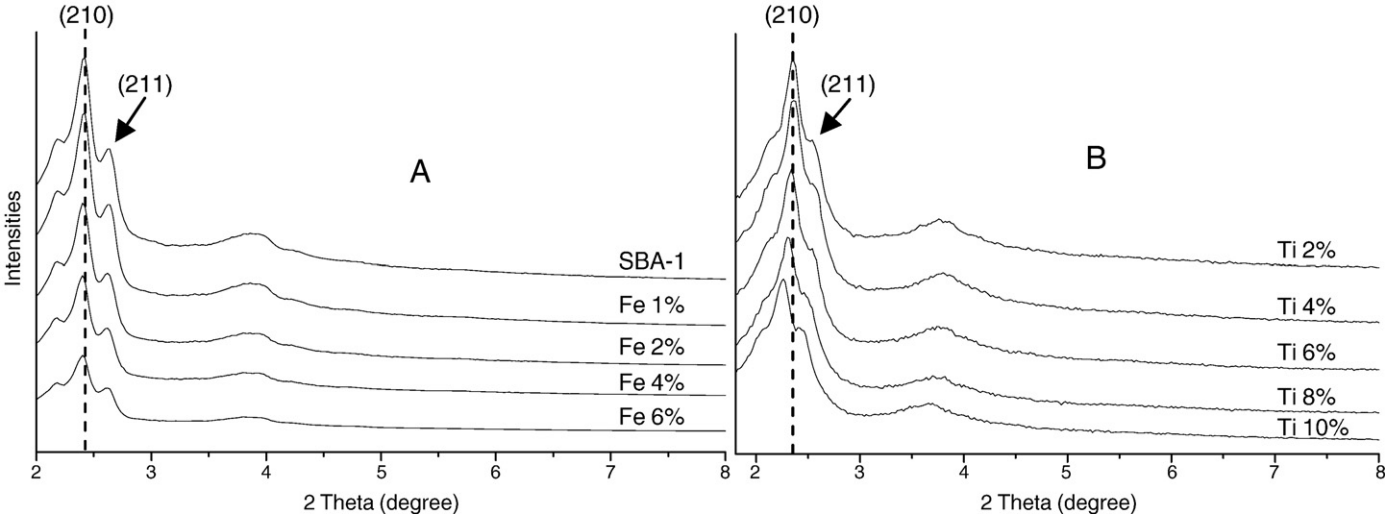


**Fig. 3.** XRD patterns of calcined Fe-SBA-1 (A) and Ti-SBA-1 (B) containing different metal loadings.

**Table 1**
Physical and crystallographic characteristics of M-SBA-1 (M=$Fe^{3+}$, $Ti^{4+}$) mesoporous materials as a function of metal loading

| Material | | Physical properties | | | Crystallographic properties | |
|---|---|---|---|---|---|---|
| Designation | Metal Doping (wt.%) | BET surface area ($m^2/g$) | Pore volume ($cm^3/g$) | Average pore diameter (nm) | $d_{210}$ (nm) | $a_0$ (nm) |
| SBA-1 | 0 | 1435 | 0.75 | 2.12 | 3.62 | 8.09 |
| Fe 2% | 2 | 1164 | 0.61 | 2.11 | 3.65 | 8.16 |
| Fe 4% | 4 | 1175 | 0.61 | 2.11 | 3.68 | 8.23 |
| Fe 6% | 6 | 1062 | 0.54 | 2.10 | 3.71 | 8.30 |
| Ti 2% | 2 | 1101 | 0.57 | 2.07 | 3.77 | 8.43 |
| Ti 4% | 4 | 1029 | 0.56 | 2.17 | 3.80 | 8.51 |
| Ti 6% | 6 | 880 | 0.51 | 2.34 | 3.83 | 8.58 |

[a]Lattice parameters $a_0$ were calculated based on the formula $a_0=\sqrt{5}d_{210}$.

TEA molecules that act as a co-template in mesoporous formation, and in addition, reduce the net positive charge on silica [15] to enhance the interaction with metal ions and promote higher metal incorporation in SBA -1.

Diffuse reflectance UV–visible spectroscopy was used to characterize the nature and coordination of $Fe^{3+}$ [3] and $Ti^{4+}$ ions [12] in the SBA-1 mesoporous molecular sieves. Fig. 1 (A and B) shows UV–visible spectra of the calcined Fe-SBA-1 and Ti-SBA-1 as a function of metal loading. For Fe-SBA-1, all samples showed a strong UV band at ~230 nm associated with a shoulder at 290 nm consistent with Laporte-allowed ligand-to-metal charge transfer involving isolated $Fe^{3+}O_4$ co-ordination [3]. The intensity of these bands increases monotonically with Fe content, as expected if there is crystallographic incorporation of Fe in SBA-1. A characteristic band above 320 nm typical of octahedral co-ordination ($Fe^{3+}O_6$) was absent indicating these materials are free of ferric oxide species similar to those found in iron hydroxide, iron oxyhydroxide and iron oxide [18–20]. The Ti-SBA-1 samples show an absorption band centered at 220 nm characteristic of the charge-transfer transition associated with regular $Ti^{4+}O_4$ framework tetrahedra. Octahedral co-ordination ($Ti^{4+}O_6$) is unlikely as the distinctive feature at 330 nm is missing [11,12].

The X-band ESR spectra of the calcined Fe-SBA-1 (Fig. 2) shows two major components at $g$=4.3, assigned to high-spin $Fe^{3+}$ in a distorted tetrahedral environment, and $g$=2.0, attributed to high-spin $Fe^{3+}$ in a symmetrical tetrahedral/octahedral coordination [3]. With increasing iron content, the corresponding ESR signals increase in intensity. The observation of the $g$=2.0 signal alone cannot be taken as unambiguous evidence for iron framework substitution unless combined with other physical or chemical methods, because of possible contributions from extra-framework $Fe^{3+}$ [20–22].

Small angle XRD confirmed that after calcination, ordered mesopores were obtained regardless of the metal (Fe/Ti) loading (Fig. 3). SBA-1 displays three well resolved diffraction peaks in the region of $2\theta$= 1.5–3° which can be indexed as (200), (210) and (211) reflections with respect to a cubic lattice [11,18], that persists to an iron loading of 6 wt.% (Fig. 3A). A similar trend was observed to the Ti-loaded samples (Fig. 3B) although the reflections are somewhat broader. Dilation of the $d_{210}$ spacing of Ti-SBA-1 with increasing titanium loading confirms the substitution of titanium ($Ti^{4+}$=0.42 Å) for silicon ($Si^{4+}$=0.26 Å) in the framework [12–14].

Since the radius of the ionic $Fe^{3+}$ is larger than that of $Si^{4+}$ ($r^{3+}_{Fe}$=0.49 Å and $r^{4+}_{Si}$=0.26 Å), dilation of $a_0$ (Table 1) is consistent with $Fe^{3+}$ incorporation in the SBA-1 framework [3]. However, the decrease in intensity of the (200) and (211) reflections, with an increasing iron content, suggests a reduction in the degree of ferrosilicate polymerization and structural order [18]. Generally, it is expected that the unit cell parameter will be enlarged after the incorporation of metal cations with ionic radii larger than $Si^{4+}$.

Transmission electron microscope lattice images (Fig. 4A and B) of representative Ti-SBA-1 and Fe-SBA-1 crystals demonstrates that regular mesopore arrays had formed, and exclude the presence of metal segregation, as this would be readily detected due to the greater electron scattering powder of Fe/Ti compared to Si.

The $N_2$ adsorption/desorption isotherms of calcined Fe- and Ti-SBA-1 were all type IV (not shown) and showed steep increases in the volume of adsorbed nitrogen at relative pressures of $P/P_0$=0.1–0.3 due to the onset of capillary condensation within uniform mesopores [15]. Both Fe- and Ti-SBA-1 possessed a narrow pore size distribution with an average pore diameter of ~2 nm confirming the TEM observations. The incorporation of higher metal contents decreases the specific surface area from 1435 to 880 $m^2/g$.

## 4. Conclusions

Silatrane obtained from the Oxide One Pot Synthesis (OOPS) process is a highly reactive precursor for the preparation of transition metal-bearing SBA-1 mesoporous materials. It has been demonstrated that the SBA-1 framework can accommodate up to 6 wt.% Fe and 10 wt.% Ti without perturbing mesopore order. Dilation of the mesoporous lattice with metal loading is consistent with crystallochemical framework replacement of $Si^{4+}$ by $Fe^{3+}/Ti^{4+}$ and the predominant retention of the metals in tetrahedral co-ordination to oxygen. However, to maintain charge balance as $Fe^{3+}$ replaces $Si^{4+}$ some edge-sharing octahedral $FeO_6$ clusters may be present as suggested by ESR spectroscopy.

## Acknowledgements

This research work is financially supported by the Postgraduate Education and Research Program in Petroleum and Petrochemical Technology (ADB) Fund, the Ratchadapisake Sompote Fund, Chulalongkorn University and the Thailand Research Fund (TRF).

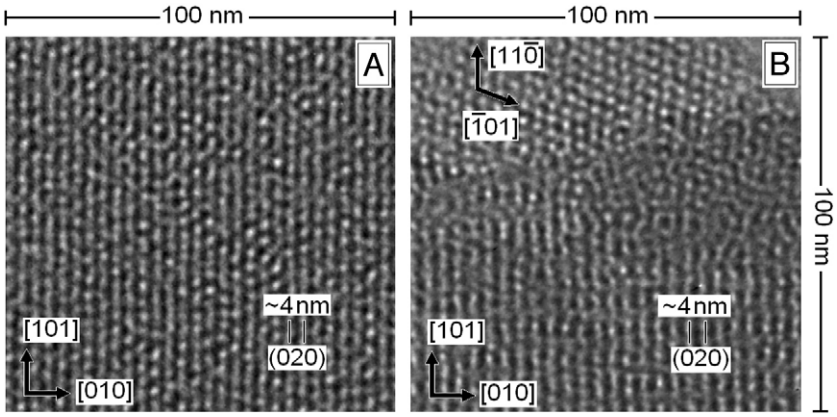


**Fig. 4.** Typical bright field TEM images of calcined M-SBA-1 at Fe 4% (A) and Ti 4% (B) metal loadings. The imaging conditions are selected so that white dots indicate connected cavities columns, with the micrographs labeled according to a cubic cell, and orientated in [−101]. Ordering is well developed along [010], but less so in [101], and for all materials, commonly extended for several nanometres. In the upper part of (B) a [111] crystal fragment extends under the [−101] fragment to create a Moiré interference pattern, confirming the mesopore order of each part.

## References


[1] Bordiga S, Buzzoni R, Geobaldo F, Lamberti C, Giamello E. J Catal 1996;158:486–501.
[2] Vinue A, Krithiga T, Murugesan V, Hartmann M. Adv Mater 2004;16:1817–21.
[3] Vinu A, Krithiga T, Gokulakrishnan N, Srinivasu P, Anandan S, Agira K. Micropor Mesopor Mater 2007;100:87–94.
[4] Selvaraj M, Pandurangan A, Seshadri KS, Sinha PK, Krishnasamy V, Lal KB. J Mol Catal A: Chem 2002;186:173–86.
[5] Jana SK, Takahashi H, Nakamura M, Kaneko M, Nishida R, Shimizu H. Appl Catal A: Gen 2003;245:33–41.
[6] Huo Q, Margolese DI, Ciesla DI, Demuth DG, Feng P, Gier TE. Chem Mater 1994;6:1176–91.
[7] Vinu A, Dedecek J, Murugesan V, Hartmann M. Chem Mater 2002;14:2433–5.
[8] Zhao X, Wang X. J Mol Catal A: Chem 2007;261:225–31.
[9] Dai LX, Teng YH, Tabata K, Suzuki E, Tatsumi T. Micropor Mesopor Mater 2001;44–45:573–80.
[10] Dai LX, Tabata K, Suzuki E, Tatsumi T. Chem Mater 2001;13:208–12.
[11] Ji D, Ren T, Yan L, Suo J. Mater Lett 2003;57:4474–7.
[12] Rajakovic VN, Mintova S, Senker J, Bein T. Mater Sci Eng C 2003;23:817–21.
[13] Anand R, Hamdy MS, Gkourgkoulas P, Maschmeyer Th, Jansen JC, Hanefeld U. Catal Today 2006;117:279–83.
[14] Thanabodeekij N, Tanglumlert W, Gulari E, Wongkasemjit S. Appl Organomet Chem 2005;19:1047–54.
[15] Tanglumlert W, Imae T, White TJ, Wongkasemjit S. J Am CeramSoc 2007;90:3992–7.
[16] Charoenpinijkarn W, Suwankruhasn M, Kesapabutr B, Wongkasemjit S, Jamieson AM. J Eur Polym 2001;37:1441–8.
[17] Phonthammachai N, Chairassameewong T, Gulari E, Jamieson AM, Wongkasemjit S. J Met Mat Min 2002;12:23–8.
[18] Anderson MW, Egger CC, Tiddy GJT, Casci JL, Brakke KA. Angew Chem Int 2005;44:3243–8.
[19] Li Y, Feng Z, Lian Y, Sun K, Zhang L, Jia G, et al. Micropor Mesopor Mater 2005;84:41–9.
[20] Goldfarb D, Bernardo M, Strohmaier KG, Vaughan DEW, Thomann H. J Am Chem Soc 1994;116:6344–53.
[21] Selvam P, Mohapatra SK. J Catal 2006;238:88–99.
[22] Bachari K, Millet JMM, Bonville P, Cherifi O, Figueras F. J Catal 2007;249:52–8.